Neural Predictors of Motor Control and Impact of Visuo-Proprioceptive Information in Youth

Sharissa H.A. Corporaal [ID],[1] **Jolien Gooijers,**[1] **Sima Chalavi,**[1] **Boris Cheval,**[2,3]
Stephan P. Swinnen,[1] **and Matthieu P. Boisgontier** [ID][1]*

[1]*Department of Movement Sciences, Movement Control and Neuroplasticity Research Group, KU Leuven, Leuven, Belgium*
[2]*Department of General Internal Medicine, Rehabilitation and Geriatrics, University of Geneva, Geneva, Switzerland*
[3]*Swiss NCCR "LIVES - Overcoming Vulnerability: Life Course Perspectives", University of Geneva, Geneva, Switzerland*

◆ ━━━━━━━━━━━━━━━━━━━━━━━━━━━ ◆

Abstract: For successful motor control, the central nervous system is required to combine information from the environment and the current body state, which is provided by vision and proprioception respectively. We investigated the relative contribution of visual and proprioceptive information to upper limb motor control and the extent to which structural brain measures predict this performance in youth ($n = 40$; age range 9–18 years). Participants performed a manual tracking task, adopting in-phase and anti-phase coordination modes. Results showed that, in contrast to older participants, younger participants performed the task with lower accuracy in general and poorer performance in anti-phase than in-phase modes. However, a proprioceptive advantage was found at all ages, that is, tracking accuracy was higher when proprioceptive information was available during both in- and anti-phase modes at all ages. The microstructural organization of interhemispheric connections between homologous dorsolateral prefrontal cortices, and the cortical thickness of the primary motor cortex were associated with sensory-specific accuracy of tracking performance. Overall, the findings suggest that manual tracking performance in youth does not only rely on brain regions involved in sensorimotor processing, but also on prefrontal regions involved in attention and working memory. *Hum Brain Mapp* 38:5628–5647, 2017.   © 2017 **Wiley Periodicals, Inc.**

Key words: child; adolescent; motor skills; sensory feedback; brain

◆ ━━━━━━━━━━━━━━━━━━━━━━━━━━━ ◆

INTRODUCTION

Many daily tasks require the use of both hands simultaneously (e.g., getting dressed, using scissors, and tying shoelaces). Young children are often unable to perform these bimanual tasks efficiently. For example, it has been shown that infants up to 12-months old fail in >50% of their attempts in a toy-retrieval task requiring them to take a toy from a lid-closed transparent box [Birtles et al., 2011]. Between 12 and 18 months, children adopt a sequential coordination strategy in which only one hand is

controlled at once. This strategy improves with age towards differentiated and simultaneous hand use [Birtles et al., 2011]. In general, bimanual coordination tasks become more accurate across childhood and adolescence, regarding both temporal and spatial coupling [De Boer et al., 2012].

Sensorimotor processes required for the perception of position (i.e., position sense or statesthesia) and movement (i.e., movement sense or kinesthesia) are thought to be critical for refining bimanual coordination as they underlie the creation of proper motor plans [De Boer et al., 2012; Swinnen and Wenderoth, 2004]. To characterize position sense, studies have used joint position matching tasks [Goble et al., 2005; King et al., 2010]. Results showed that position sense is facilitated by higher accuracy of sensory systems providing information on limb position (e.g., vision and proprioception). However, the relative contribution of these different systems is not equal [Goble and Brown, 2008]. In children, visual information has been shown to contribute more than proprioceptive information to joint position sense [Gomez-Moya et al., 2016; Kagerer and Clark, 2014]. More specifically, King et al. [2010] tested children aged 7–13 years in goal-directed unimanual movements. Movement accuracy was compared between unimodal sensory conditions (visual or proprioceptive feedback) and an incongruent combined sensory condition (i.e., spatial information on the target location provided by vision did not match the information provided by proprioception). Results showed that when participants were more accurate in the unimodal proprioceptive feedback condition, they also converged less towards the (incorrect) visual location during the incongruent combined sensory condition. Based on these results, the authors suggested that the relative contribution of vision or proprioception in goal-directed movements neither depends on the 'most dominant' sensory source, nor are these sources equally weighted. Rather, it was suggested that the relative contributions of vision and proprioception depend on the accuracy of each individual sensory modality. Thus, when one modality was considered more accurate than the other, it would contribute more to movement execution. Critically, this sensory weighting was independent of age, indicating that sensory contributions were weighted according to their accuracy across all ages.

King et al. [2010] additionally showed that the relative contribution of proprioception to the multisensory target estimate was smaller in younger children compared with older children, suggesting superiority of visual over proprioceptive accuracy in the younger children. These findings were supported by the work of Kagerer and Clark [2014], showing that younger children aged 5–6 years did not use proprioceptive information as efficiently as older children aged 7–15 years. In their study, children were required to perform unimanual goal-directed movements from visually presented start positions towards target positions. During this task, visual feedback on the

movement trace could deviate 60° counterclockwise. Thus, children had to 'ignore' proprioceptive feedback of the movement trace, and instead had to make use of visual feedback to position the 'manipulated' movement trace into the target position. This required a reweighting of the visuo-proprioceptive contributions to estimate limb position. After this manipulation, visual feedback of the movement trace was removed. This required re-adaption of the sensory contributions, solely based on proprioceptive feedback. The results showed that the younger children did not re-adapt, while the older children did. Thus, the younger children were restricted to the movement mode they obtained when vision was last available and were not able to use the proprioceptive feedback to move to the targets accurately. Similar results were found by Gomez-Moya et al. [2016], who used prism-goggles to manipulate visual feedback in a group of children aged 4–12 years during a throwing task. Results showed that the younger children re-adapted significantly slower to the normal situation after removing the prism goggles than the older children. From these studies, we inferred that children older than 7–8 years of age use both vision and proprioception to control their movements, but the relative contribution of each sensory channel depends on its individual functioning. How and to which extent these two sensory modalities determine manual control in children older than 9 years is still unclear at best. Therefore, the objective of this study was to investigate the impact of visual and proprioceptive information on motor control in youth. To this end, we used a bimanual tracking task in different sensory conditions.

In addition, no study has yet investigated the brain predictors of manual control in children under different visuo-proprioceptive conditions. Here, we assumed that reciprocal interhemispheric transfer of sensory information was crucial for the execution of our bimanual tracking task. Therefore, we investigated the extent to which brain regions that were previously associated to bimanual motor control predicted motor control under different sensory conditions. Key brain regions of the motor network contributing to manual control are primary sensorimotor cortices (i.e., the primary motor cortex [M1] and primary somatosensory cortex [S1]), and lateral and medial premotor cortices (i.e., the premotor cortex (PMC) and supplementary motor area [SMA]) [Grefkes et al., 2008; Immisch et al., 2001; Jancke et al., 2000; Koeneke et al., 2004; Liu et al., 2002; Nachev et al., 2008; Swinnen and Wenderoth, 2004; Toyokura et al., 1999, 2002]. Particularly, SMA activity is more prominent during bimanual than unimanual coordination [Jancke et al., 2000; Toyokura et al., 2002] and is associated with encoding sequential movements and the inhibition of unwanted movements [Nachev et al., 2008]. The PMC is subdivided into the dorsal (PMd) and ventral part (PMv), with PMd being predominantly activated during bimanual coordination [Swinnen and Wenderoth, 2004]. Additionally, in complex motor tasks requiring attention and

cognitive control, the dorsolateral prefrontal cortex (DLPFC) is known to regulate movement preparation and execution [Beets et al., 2015; Fujiyama et al., 2016; Fuster, 2001; Lucci et al., 2014; Miller and Cohen, 2001; Pochon et al., 2001; Remy et al., 2008]. Homologous key regions in both hemispheres communicate through the corpus callosum (CC), which is crucially involved in regulating bimanual coordination [Gooijers and Swinnen, 2014; Jarbo et al., 2012].

Here, we investigated the relative contribution of visual and proprioceptive information to manual motor control and the extent to which key brain regions predict this sensory-specific control in youth. To this end, participants older than 8 years performed a bimanual tracking task according to in-phase and anti-phase coordination modes while different sources of sensory information were available. We expected tracking performance to improve with age in both coordination modes, as both sensory modalities are likely to refine over time during development. Previous work in adults has demonstrated that in-phase tracking performance was most optimal when proprioceptive information was available, while visual information appeared more critical for anti-phase tracking performance [Alaerts et al., 2007]. Based on the dominant use of visual over proprioceptive feedback in youth [Gomez-Moya et al., 2016; Kagerer and Clark, 2014; King et al., 2010], we hypothesized that visual information may interfere with proprioceptive information in youth, especially during in-phase tracking for which proprioception is most critical. Such interference would require greater involvement of controlled processes in the task to reach optimal performance. Particularly, we therefore hypothesized that brain regions involved in controlled processes of movement, that is, prefrontal structures, are stronger predictors of performance, than other regions of interest (ROIs) for bimanual tracking performance in youth. We suggested that this would be reflected by a positive effect of white matter (WM) microstructural organization, cortical surface, and cortical thickness of prefrontal structures on tracking performance.

METHODS

Participants

Forty healthy volunteers participated in this study (20 females; age range 9.0–18.9 years; mean age ± SD 14.5 ± 2.8). Participants were all right-handed as measured with the Edinburgh Handedness Questionnaire (77 ± 20%) [Oldfield, 1971]. Participants reported no neurological, muscular or cognitive disorders and were screened for MRI compatibility (i.e., no MRI-incompatible implants, dental braces, claustrophobia). The protocol was in accordance with the Declaration of Helsinki [1964] and was approved by the local ethics committee of the KU Leuven, Belgium. Participants were financially compensated for participation and both the participants and their parents provided written informed consent prior to the experiment.

Behavioral Procedure and Analyses

Apparatus and Setup

Tracking accuracy was assessed using an apparatus that has been described in detail previously in Alaerts et al. [2007] and Boisgontier et al. [2014]. In short, the hands were inserted in two manipulanda, while the forearms rested in neutral prosupination, with elbows at 90° flexion (Fig. 1). The right wrist was passively moved by an AC servo motor (AMK DV764, Goedhard PMC, Helmond, NL), mounted underneath the right manipulandum and coupled to its rotating shaft via a 1:10 reducer (Alpha Gearbox, Type LP120). This motor generated a continuous semi-random sinusoidal motion of a programmable amplitude and duration, allowing motion of the wrist from −30° (extension) to +30° (flexion), relative to a 0° position, whereby the forearm and the palmar surface of the hand were aligned. The left manipulandum was constructed similarly but enabled free flexion-extension motion of the wrist. Shaft encoders were connected to the rotating axis of both manipulanda (accuracy = 0.088°) to record angular displacement of the left and right wrist. Data were sampled at 1000 Hz (Signal software 4.0; Cambridge Electronic Design, Cambridge, UK) and low-pass filtered (second-order Butterworth, cut-off frequency at 8 Hz, zero-lag). The angular displacement signals of the manipulanda (Fig. 2) were stored for further analysis.

Procedure

The participants were instructed to track the imposed movement of the right wrist (by means of a torque motor) with their left wrist as accurately as possible, taking amplitude, velocity, and coordination mode into account. This task was performed according to two coordination modes (anti-phase and in-phase). In the anti-phase mode, participants were to track the imposed movement in the same extrinsic direction as the target manipulandum. In the in-phase mode, the movement was to be tracked 'mirror symmetrical', or symmetrically relative to body-midline. The sensory information available on the right (passively moved) wrist was manipulated using four different sensory conditions (VIS + PROP, PROP, VIS, and ATT) (Fig. 1). In the VIS + PROP condition, both visual and proprioceptive information on the participant's right wrist were available. Here, participants fixated on their right wrist throughout the trials (directing overt attention towards the right wrist). In the PROP condition, a carton box covered the right hand, providing only proprioceptive information on the right wrist. The participants were instructed to fixate on the center of the right carton box, forcing overt attention towards the right wrist. In the VIS condition, only visual information on the right wrist was available. To remove proprioceptive information in this condition, the participants laid their right hand in a relaxed position on their lap, while a third person put his/her right hand into the manipulandum. The participants were instructed
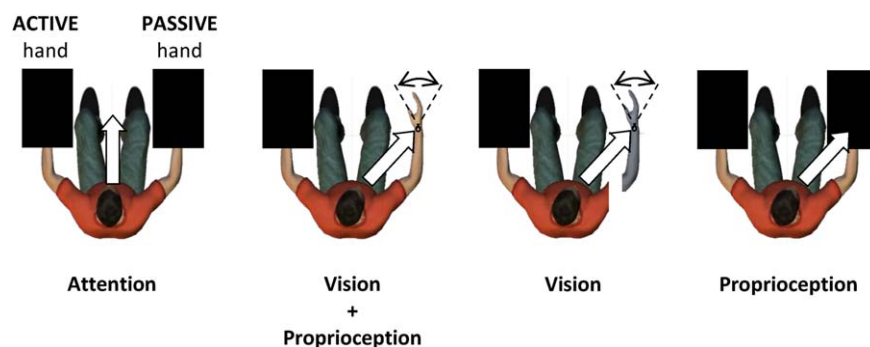
Figure 1.

Top view of the experimental setup in the ATT, VIS + PROP, VIS and PROP conditions. In all conditions, participants were instructed to track a motor-driven right-hand movement (passive) with their left hand (active). Wrist movements ranged from 30° extension to 30° flexion (dashed lines). In all conditions, vision of the left hand was occluded by covering the hand by an opaque box, here presented as a black rectangle. In the VIS + PROP condition, both visual and proprioceptive information was available from the right (passive) hand. In the VIS condition, proprioceptive information on the right (passive) hand was removed by using an alien hand (shown in gray) instead of the participant's own hand. In the PROP condition, visual information was removed by covering the right (passive) hand with an opaque box. White arrows indicate the gaze direction toward the right passive hand [adapted from Boisgontier et al., 2014]. [Color figure can be viewed at wileyonlinelibrary. com]

to fixate on this 'alien hand'. In these three sensory conditions, participants were required to direct overt attention towards the passively moved right wrist and away from the actively moved left wrist. To account for possible effects of overt attention on proprioceptive accuracy [Boisgontier et al., 2014], we included the attention condition (ATT). This condition was identical to the PROP condition, except that participants had to direct overt attention away from the passive limb by fixating on a cross located at 1 m in front of them at eye-height. By comparing the ATT with the PROP condition, the effect of overt attention on tracking performance could be evaluated. In all conditions (VIS, PROP, VIS + PROP and ATT) an opaque carton box covered the left (active) hand, thereby removing visual information.

In total, eight conditions were tested (two coordination modes × four sensory conditions). The two coordination modes were performed in two distinct blocks and the starting coordination mode was counterbalanced across participants. The sensory conditions were performed in a randomized order. Each condition consisted of four trials, each lasting 30 s. These four trials consisted of four different sinusoidal movements presented in a randomized order to prevent anticipation. The quasi-random character of each of the displacement series was ensured by continuously varying the amplitude between −30° and +30°. In total, 32 trials were recorded per participant (2 coordination modes × 4 sensory conditions × 4 trials). Prior to the recorded trials in the in-phase and anti-phase blocks, three practice trials were performed in which visual and proprioceptive information on both wrists was available. Additionally, prior to each sensory condition block, a practice trial was performed. A short break (5 min) was inserted after every eighth experimental trial.

During the experiment, participants were instructed to fully relax their right arm. Electromyographic recordings of the right flexor and extensor carpi radialis were used to monitor muscle activity (MESPEC8000 EMG system, Mega Electronics Ltd., Finland). The experimenter used the real-time EMG signal output to confirm muscle relaxation, and reminded the participant to relax their arm if needed.

Analysis of Tracking Performance

Temporal accuracy of tracking performance was calculated by taking the root mean square of the relative phase between the left and right wrist (phase error). Relative phase was defined as the subtraction of the phase angle of the left (actively moved) from the right (passively moved) wrist according to the following formula:

$$\Phi = \theta_{RW} - \theta_{LW} = \tan^{-1}\left[\frac{(dX_{RW}/dt)}{X_{RW}}\right] - \tan^{-1}\left[\frac{(dX_{LW}/dt)}{X_{LW}}\right]$$

where θ_{RW} and θ_{LW} refer to the phase of the right and left wrist movement in each sample, as obtained from the instantaneous phase derived from the Hilbert transformed signal [Boashash, 1992a,b; Carson et al., 2002] X_{RW} and X_{LW} are the position of the right and left wrist after rescaling to the interval [–1, 1] for each cycle of oscillation, and dX_{RW}/dt and dX_{LW}/dt are the normalized instantaneous velocities.

Subsequently, we calculated the root mean square (RMS) of the relative phase. The RMS is an error measure of the observed phase (θ) relative to the target phase (0° for anti-phase tracking and 180° for in-phase tracking). RMS error, also called total error, is a combination of the
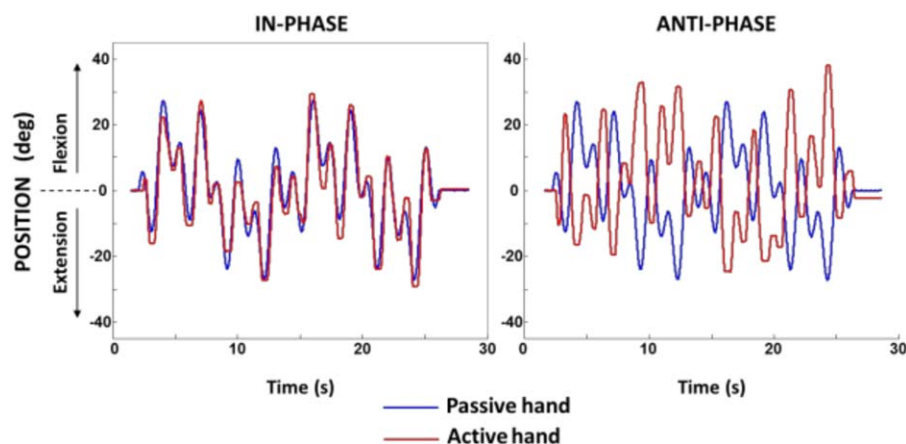
Figure 2.

Sample of motor-generated motion in the passive hand and tracking motion of the active hand for in-phase and anti-phase conditions [adapted from Boisgontier et al., 2014]. [Color figure can be viewed at wileyonlinelibrary.com]

constant error (CE) and the variable error (VE) as in $E^2 = CE^2 + VE^2$. Conversely, the absolute error does not equally incorporate CE and VE, which may result in an ambiguous interpretation of the performance (Chai and Draxler, 2014). RMS error of the relative phase was therefore preferred as an indicator of phase error.

Image Acquisition and Analyses

Image Acquisition

A Philips Ingenia 3T CX MRI scanner with a standard 32-channel head coil was used for image acquisition. For all participants, a high-resolution T1-weighted structural image was acquired for anatomical detail, using MPRAGE (TR = 9.71 ms, TE = 4.60 ms, $0.98 \times 0.98 \times 1$ mm^3 voxels, field of view = 210.94×230 mm^2, 230 sagittal slices). Additionally, single-shell diffusion weighted images (DWI) were acquired using the following parameters: single-shot spin echo, slice thickness = 2.5 mm, TR = 7,600 ms, TE = 65 ms, number of diffusion directions = 60, number of sagittal slices = 58, voxel size = $2.5 \times 2.5 \times 2.5$ mm^3, diffusion weighting of $b = 1,300$, one non-diffusion weighted image.

Diffusion Weighted Image Processing and Probabilistic Tractography

We used diffusion tensor imaging (DTI) to visualize cerebral WM, and make inferences on WM microstructural architecture. DTI determines the distinct diffusion patterns of water molecules that are found in different tissue types in the brain (e.g., WM and gray matter [GM]) [Basser and Jones, 2002]. The amount and directionality of the diffusion of water molecules is described by mean diffusivity (MD) and fractional anisotropy (FA), respectively [Basser, 1997; Basser et al., 1994; Beaulieu, 2002; Beaulieu and Allen, 1994; Emsell et al., 2016; Le Bihan, 1995]. FA represents the degree of anisotropy of diffusion in a voxel. FA is a rotationally invariant index, which ranges from 0 (isotropic) to 1 (anisotropic). Lower MD values and higher FA values indicate more anisotropic motion of water molecules, reflecting a more coherent organization of WM microstructure [Basser and Pierpaoli, 1996].

Image pre-processing. We performed quality checks on each diffusion-weighted imaging volume using Explore DTI [Leemans et al., 2009]. As recommended by Tournier et al. [2011], we inspected the volumes in three orthogonal views (sagittal, coronal, frontal) to identify visible artifacts, such as large signal dropouts and geometric distortions. When an artifact (anything, except motion-related) was detected in an isolated volume, this volume was removed. In 8 participants, isolated volumes were removed due to artifacts that were not related to head movements. In volumes where head movements of more than 2 mm translation and/or 2° rotation occurred, all assembled volumes that were collected after the movement onset were removed, while making sure that at least two-third of volumes remained. All movement corrections stayed within this limit, thus no participants were excluded from analyses due to movement artifacts.

After the quality checks, diffusion-weighted data were further preprocessed using the FMRIB (Functional MRI of the Brain) Software Library, FSL (Oxford University, Oxford, UK; www.fmrib.ox.ac.uk/fsl). For each participant, eddy-current-induced geometric distortions and head movements were corrected. Then, the diffusion-weighted volumes were corrected for distortions resulting from magnetic field inhomogeneities using fieldmap correction and were aligned to their corresponding non-diffusion-weighted (b0) image. The gradient direction table

was adjusted to account for rigid transformations resulting from motion and eddy current corrections.

Cortical ROIs and seed masks. We selected key regions of the motor network that have also been shown to be involved in bimanual motor control: S1, M1, pre-SMA, SMA proper, and PMd [Debaere et al., 2004; Naito, 2004; Nachev et al., 2008; Swinnen and Wenderoth, 2004]. In addition to these key regions, we selected the DLPFC as an important frontal region executing cognitive control over bimanual coordination. The DLPFC integrates information stored in the working memory to organize upcoming actions [Fuster, 2001; Miller and Cohen, 2001; Lucci et al., 2014; Pochon et al., 2001], and is involved during movement preparation [Fujiyama et al., 2016] and execution [Beets et al., 2015; Remy et al., 2008] of more complex bimanual tasks.

Six cortical seed masks of interest (i.e., starting points from which tracts were generated) were created in FSL for probabilistic tractography: M1, S1, pre-SMA, SMA proper, PMd, and DLPFC (Fig. 3a). For M1 and PMd, we used the Human Motor Area Template (http://lrnlab.org/) [Mayka et al., 2006]. S1 was created by combining the Brodmann areas 2, 1, 3a, and 3b [Geyer et al., 2000; Grefkes et al., 2001] from the Jülich Histological Atlas. The masks for pre-SMA and SMA proper were created by the AAL template [Tzourio-Mazoyer et al., 2002], divided by a vertical line through the anterior commissure (i.e., $y > 0$) [Smith et al., 2004]. For DLPFC, we first extracted the middle frontal gyrus (MFG) from the Harvard-Oxford Cortical Structural Atlas [Desikan et al., 2006; Frazier et al., 2005; Goldstein et al., 2007; Makris et al., 2006]. The most anterior half of the MFG was determined as the DLPFC [Smith et al., 2004]. Additionally, a waypoint mask of the CC was used to restrict tractography to those fibers passing through the CC. The CC is the largest WM structure connecting homologous cortical regions of the two hemispheres, and to a lesser extent heterologous regions [Jarbo et al., 2012]. The crucial contribution of the CC to bimanual coordination has been widely demonstrated [for a review see Gooijers and Swinnen, 2014].

Using Tract-Based Spatial Statistics of FSL [Smith et al., 2004, 2006], FA and MD images were created by fitting a tensor model to the raw diffusion data using FMRIB's Diffusion Toolbox, and then brain-extracted using the Brain Extraction Tool [Smith, 2002]. The FA and MD values of all participants were then aligned into a common space (FMRIB58_FA) using the non-linear registration tool FNIRT (http://www.fmrib.ox.ac.uk/analysis/techrep/tr07ja2/tr07ja2.pdf), which uses a b-spline representation of the registration warp field. The inverse warping matrix of the registrations generated during this previous step was used to warp the seed masks to native subject spaces.

Constrained spherical deconvolution and probabilistic tractography. Tractography between seed masks was performed with the MRtrix 0.2.12 software package [http://www.brain.org.au/software; Tournier et al., 2012]. For this, a mask was extracted from each individual eroded MD and FA map. The FA mask was created by extracting predominantly voxels containing a single fiber (choosing only strongly anisotropic voxels with FA > 0.7) to estimate the spherical-harmonic coefficients of the response function [Tournier et al., 2004, 2008]. Then, the fiber orientation distribution (FOD) was estimated at a whole-brain level by means of constrained spherical deconvolution (CSD) of the diffusion-weighted signal. This procedure is based on the assumption that the diffusion-weighted signal measured from any fiber bundle is adequately described by a single-response function [Tournier et al., 2004]. This method has shown to provide FOD estimates robust to noise while preserving angular resolution and allowing proper tracking in regions of crossing fibers [Tournier et al., 2004, 2007, 2008, 2011, 2012]. CSD was performed with the maximum harmonic order set to 8. Subsequently, probabilistic fiber tracking was conducted between seed masks of the M1, S1, pre-SMA, SMA proper, PMd, and DLPFC, which reconstructed bilateral tracts connecting these regions based on an algorithm that uses the fiber orientation at each step. Any tract connecting these cortical regions via the CC was included in the reconstructed tracts. The following parameters were used for the tracking algorithm: step size of 0.2 mm, radius curvature of 1 mm, maximum tract length of 200 mm, and FOD cutoff value of 0.1.

At this point, tracts were created for each participant between the seed masks (Fig. 3b). To perform an accurate comparison of the FA and MD values of these tracts between participants, only the voxels of the tracts that were shared by the majority of the participants were selected. To this end, we first warped the tracts of each participant to common space (MNI, Montreal Neurological Institute) in MRtrix. Subsequently, we created tract density maps that hold measures of the fraction of tracts entering each voxel. Of these maps, we created binary masks, by including all voxels with ≥ 1 tract entering. Next, we combined the binary masks per tract of all participants, and then selected only those voxels that were shared by $\geq 82\%$ of the participants (absolute $n = 33$). These masks, now including only the voxels shared by the majority of the participants, were inverse warped to subject space, and FA and MD values of these common voxels were extracted for each participant. Subsequently, mean FA and MD values for each interhemispheric tract were obtained by averaging the FA and MD values of all voxels within a tract (using the mrstats function in MRtrix). This resulted in one mean FA and MD value per tract per participant.

Cortical GM Surface and Thickness

To complement the results based on the microstructural organization of WM tracts, we assessed whether cortical thickness and surface area (GM metrics) contributed to bimanual tracking performance in youth. Although cortical thickness and surface area are the product of independent
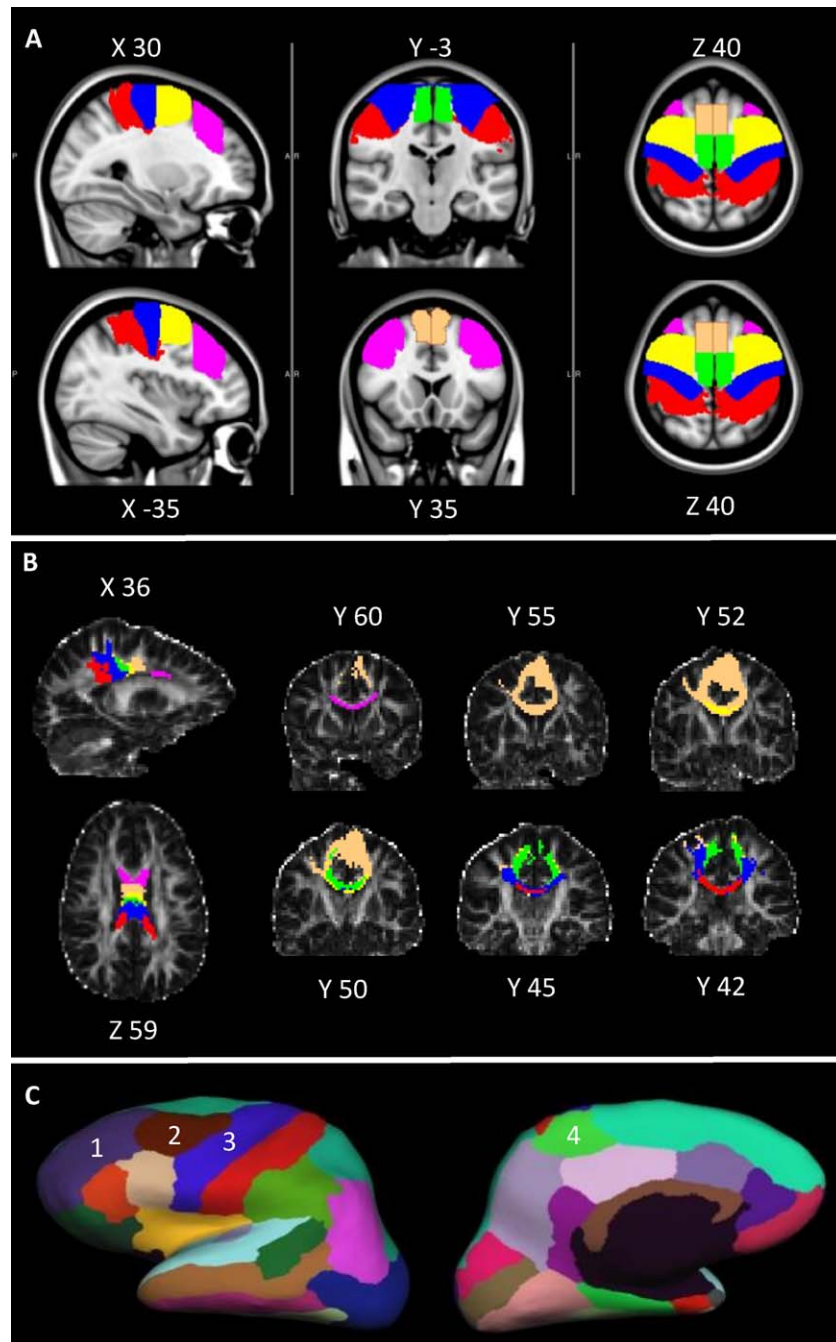
Figure 3.

Overview of cortical ROIs. **(A)**. FSL's cortical masks used for probabilistic CSD tractography, displayed onto a standard MNI template. Shown are the DLPFC (pink), PMd (yellow), M1 (blue), S1 (red), SMA (proper; green) and pre-SMA (copper). **(B)** Microstructural characteristics (FA and MD) of interhemispheric tracts were only obtained from voxels that were shared by >85% of the participants. Here, voxels are displayed in subject space of a representative participant. **(C)** Lateral (left panel) and medial (right panel) view of the cortical parcellation of the Desikan-Killiany atlas [Desikan et al., 2006], displayed on an inflated template (https://surfer.nmr.mgh.harvard.edu). FreeSurfer's cortical masks used for GM analyses were selected based on their overlap with FSL's masks of critical tracts for bimanual tracking performance: rostral (1; purple) and caudal middle frontal cortex (2: brown) (both overlapping with FSL's mask for DLPFC), precentral cortex (3; blue) (overlapping with FSL's mask for M1), and paracentral cortex (4; green) (overlapping with FSL's mask for SMA proper). [Color figure can be viewed at wileyonlinelibrary.com]

neurobiological processes [Panizzon et al., 2009], both are thought to reflect characteristics of the population of neural cells within the cortex. The surface area is thought to represent the number of cell columns with a shared ontogenetic origin, whereas the cortical thickness represents the number and/or size of neural cells within a column [Panizzon et al., 2009; Rakic, 1988, 2007]. Both measures (cortical thickness and surface area) have previously been linked to cognitive performance, such as working memory, attention and set-shifting, in which thinner and smaller cortices were correlated to poorer cognitive functioning [Gautam et al., 2015; Haring et al., 2016; Langevin et al., 2015; Salthouse et al., 2015; Shaw et al., 2006; Tuladhar et al., 2015).

Cortical reconstruction and volumetric segmentation were performed with the FreeSurfer image analysis suite (v5.1; http://surfer.nmr.mgh.harvard.edu/). Two cortical measures were extracted from the T1-weigthed images: cortical surface (mm^2) and cortical thickness (mm). Details of these procedures were described in prior publications [Dale et al., 1999; Fischl and Dale, 2000; Fischl et al., 2002, 2004a,b]. Briefly, this processing included motion correction of the raw T1-weigthed images (Reuter et al., 2010), brain extraction, and Talairach transformation. Then, WM and GM were segmented [Fischl et al., 2002, 2004a,b] and intensity inhomogeneities were normalized [Sled et al., 1998]. The GM/WM boundary was tesselated and the surface was deformed following intensity gradients to optimally place the GM/WM and GM/cerebrospinal fluids (CSFs) borders at the location where the greatest shift in intensity defines the transition to the other tissue class [Dale and Sereno, 1993; Dale et al., 1999; Fischl and Dale, 2000]. Once the cortical models were completed, a refinement procedure was applied to obtain a representation of the GM/WM boundary. This surface was subsequently deformed outward to obtain an explicit representation of the pial surface, which was then divided into distinct cortical regions. The parcellation labeled cortical sulci and gyri [Desikan et al., 2006; Fischl et al., 2004a,b], and cortical surface area and cortical thickness values were calculated in 68 cortical regions. Cortical surface area was calculated as the sum of the areas of each tessellation falling within each region. Cortical thickness was calculated as the average distance between the GM/WM boundary and the GM/CSF boundary within each region. The surface area and cortical thickness of the homologous cortical areas of the left and right hemisphere were combined into one summary measure. The surface measure was calculated by summing the individual values of the contributing brain regions, while for the thickness measure, values of the contributing brain regions were averaged.

Statistical Analyses

Linear mixed models (LMMs) were used to analyze the data. In several research fields, the use of LMM is promoted as an alternative to more traditional statistical approaches such as repeated measures ANOVA [Boisgontier and Cheval, 2016; Smith, 2012]. In addition to other advantages mentioned elsewhere (http://www.stat.cmu.edu/~hseltman/309/Book/chapter15.pdf), LMM can handle missing data and keep all data from all participants with missing observations. Additionally, LMM can include every single trial in the model, instead of averaging trials per condition, thereby preventing the loss of information and reducing the risk for Type-I errors.

Like ANOVA, LMM include both fixed and random effects to model the data. The fixed effects are the average estimates of intercepts and slopes (with numerical measures) or contrasts (with categorical measures) of both participants and conditions. The random effects represent the adjustments to intercepts and slopes/contrasts measures per individual participant. Thus, the basic idea is that fixed effect parameters represent the average differences between conditions, while random effect parameters represent the variability (around this average difference) between participants. Here, LMM were built with phase error as dependent variable. Different predictors and covariates were used for behavioral, WM, and GM investigations. All models were adjusted for gender and trial order (1–16). These models were build using the R language lmerTest package, version 1.1–7 (https://CRAN.R-project.org/package = lmerTest). The predictors were checked for the absence of multicollinearity, that is, showing variance inflation factors (VIFs) below 10 [Hair et al., 1995]. The PMd was removed due to high multicollinearity in Models 2a and 2b (VIF = 13.22) and Models 2c and 2d (VIF = 17.32). For all statistical tests, the levels of significance were set at $P < 0.05$. Finally, an estimate of the effect size was reported using the conditional pseudo R2, which was computed using the MuMin package, version 1.15–6 of the R software (https://CRAN.R-project.org/package=MuMIn).

Model 1 was designed to investigate the extent to which age, coordination mode, and sensory condition predicted tracking performance based on phase error.

Models 2 and 3 were designed to investigate the extent to which WM and GM metrics predicted behavioral performance, above and beyond the effect of age. Particularly, Models 2a-2d were designed to investigate the extent to which FA and MD predicted tracking performance (i.e., phase error). We included both fixed effects of WM tracts, and their interactions with sensory conditions. The sensory condition ATT was not included in the models, since Model 1 indicated no effect of overt attention on tracking performance. As we investigated the effects of age, coordination mode and sensory condition in Model 1, we controlled for these effects by including them as covariates in Models 2 and 3. Including age as a covariate in Models 2 and 3 allowed us to control for the variance in the outcome (i.e., phase error) that was explained by age, including the effect of age on brain structure. Therefore, any significant fixed effect or interaction effect involving brain structures indicated that these were true irrespective of

TABLE I. Behavioral performance

Fixed effects[a]	Phase error		
	b	SE	P-value
Intercept	58.431	2.602	<0.001***
Age	−8.613	1.765	<0.001***
Gender	0.503	3.460	0.885
Trial	−0.615	0.076	<0.001***
Coordination mode In-phase (ref anti-phase)	−2.390	0.694	<0.001***
Sensory condition VIS (ref ATT)	7.621	0.983	<0.001***
Sensory condition VIS+PROP (ref ATT)	−2.158	0.987	0.029*
Sensory condition VIS+PROP (ref VIS)	−9.779	0.982	<0.001***
Sensory condition PROP (ref ATT)	−1.124	0.982	0.253
Sensory condition PROP (ref VIS)	−8.745	0.981	<0.001***
Sensory condition PROP (ref VIS+PROP)	1.034	0.984	0.293
Coordination mode × Age	2.236	0.694	0.001**
Random effects	σ^2		
Participants			
Intercept	112.1		
Residual	153.8		
Effect size (R_c^2)	0.557		

[a]The reference for the fixed effects shown here is, by default, the visual condition. Sensory conditions displayed are the ATT, VIS, PROP and VIS + PROP conditions. R_c^2 conditional pseudo R^2. ***$P < 0.001$, **$P < 0.01$, *$P < 0.05$.

age, that is, that the significant effect of the structure predicts tracking performance above and beyond the effect of age.

Because the software for WM (FSL) and GM analyses (FreeSurfer) utilize different cortical atlases to label cortical brain regions, we selected the corresponding regions by visual comparison of the (partially) overlapping regions between both atlases. For this, we used the results of Model 2, which indicated which WM tracts were predictive of performance. FSL's seed masks used to reconstruct these critical WM tracts were subsequently compared with the cortical atlas used by FreeSurfer (Desikan et al., 2006) to identify the corresponding brain regions. The cortical regions in FreeSurfer, that (partly) overlapped with FSL's seed masks of the critical WM tracts, were then used as cortical masks for further investigation of GM predictors of behavior (Fig. 3c). Subsequently, Models 3a-3d were designed to investigate the extent to which cortical GM surface and GM thickness predicted manual tracking performance (i.e., phase error).

RESULTS

Behavioral Predictors

Model 1 (Table I) tested the effects of age, sensory condition, and coordination mode on phase error. The model showed that age predicted tracking performance ($b = -8.613$, SE = 1.765, $P < 0.001$), with older participants being more accurate. Coordination mode was also predictive of tracking performance ($b = -2.390$, SE = 0.694,

$P < 0.001$), with in-phase being performed with lower phase error than anti-phase. Model 1 also showed a significant coordination mode × age interaction ($b = 2.236$, SE = 0.694, $P = 0.001$) indicating that phase error decreased more from younger (mean −1 SD) to older (mean +1 SD) participants in the anti-phase ($b = -8.613$, SE = 1.765, $P < 0.001$) than in the in-phase mode ($b = -6.377$, SE = 1.765, $P < 0.001$) (Fig. 4). For sensory condition, VIS was performed with less accuracy than the remaining three conditions (PROP $b = -8.745$, SE = 0.981, $P < 0.001$; VIS + PROP $b = -9.779$, SE = 0.982, $P < 0.001$; ATT $b = -7.621$, SE = 0.983, $P < 0.001$). Performance was not different between PROP and ATT ($b = -1.124$, SE = 0.982, $P = 0.253$). Therefore, we excluded the ATT condition from further analyses.

WM Predictors

Overall, age-related changes in WM microstructural organization supported previous literature on brain maturation [Uda et al., 2015; Wu et al., 2014]. More specifically, FA values in M1, SMA proper, and pre-SMA increased with age. Correlations between age and FA values in S1 and DLPFC, and MD values in all tracts were non-significant (see Supporting Information).

Fractional Anisotropy

Model 2a (Table II) assessed the extent to which mean FA of interhemispheric homologous M1, S1, SMA proper, pre-SMA, and DLPFC tracts predicted phase error. Results
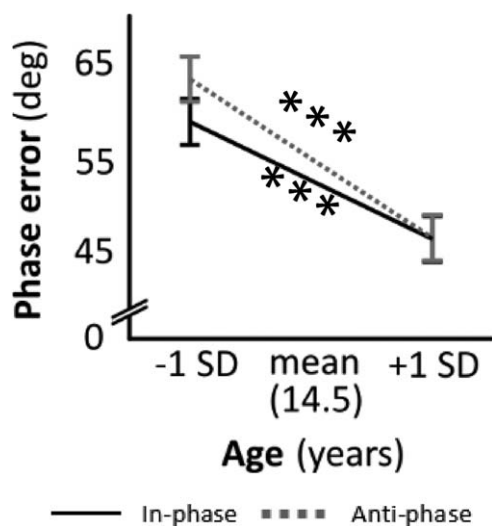
Figure 4.
Age-related effects on phase error. Significant age-related improvements of tracking accuracy were found ($P < 0.001$) in both coordination modes (i.e., in-phase and anti-phase). Additionally, while tracking accuracy was overall higher for in-phase than anti-phase coordination modes, this differentiation was most pronounced in younger participants.

showed no fixed effect of these tracts on phase error ($P > 0.05$). However, a significant interaction between M1 and PROP versus VIS ($b = -4.552$, SE $= 2.011$, $P = 0.024$) was found, as well as an interaction between SMA proper and PROP versus VIS ($b = 3.504$, SE $= 1.723$, $P = 0.042$).

To build a more parsimonious model and to confirm the sensitivity of our results, all the ROIs identified as non-significant in Model 2a were removed (Model 2b, Table II). Overall, this new model predicted the data more accurately than the original model (2a; Δ AIC $= -12.9$). The interactions between PROP versus VIS and M1 ($b = -4.181$, SE $= 1.328$, $P = 0.002$) and SMA proper ($b = 3.545$, SE $= 1.326$, $P = 0.008$) remained significant, confirming the robustness of these effects. However, within each sensory condition, simple slope analyses on the effects of FA on phase error did not reveal significant effects for these tracts (all $P > 0.05$; Supporting Information). This suggests that these interactions were not critical to disentangle the sensory-specific effect of FA on phase error.

Mean Diffusivity

Model 2c (Table II) assessed the extent to which mean MD of interhemispheric homologous M1, S1, SMA proper, pre-SMA, and DLPFC tracts predicted phase error. Results showed no fixed effects of these tracts on phase error ($P > 0.05$). However, a significant interaction between DLPFC and PROP versus VIS ($b = 3.455$, SE $= 1.483$,

$P = 0.020$) was found. To build a more parsimonious model and to confirm the sensitivity of our results, all ROIs identified as non-significant in Model 2c were removed (Model 2d, Table II). This new model predicted the data more accurately than the original model (2c; Δ AIC $= -16.4$). The interaction between DLPFC and PROP versus VIS remained significant ($b = 3.225$, SE $= 0.965$, $P < 0.001$), confirming the robustness of the effects (Fig. 5a). Simple slope analyses performed on these sensory conditions (PROP and VIS), revealed a significant effect of increasing MD on phase error in PROP (increasing phase error; $b = 4.660$, SE $= 1.781$, $P = 0.012$), but not in VIS ($b = 1.435$, SE $= 1.781$, $P = 0.424$). Additionally, in the new model (2d), a significant interaction emerged between DLPFC and VIS + PROP versus VIS ($b = 1.968$, SE $= 0.966$, $P = 0.042$). However, simple slope analyses on the effects of MD on phase error in these sensory conditions (VIS + PROP and VIS) did not reveal significant effects ($P > 0.05$). This suggests that this latter interaction was not critical to disentangle the sensory-specific effect of MD on phase error.

GM Predictors

The WM tracts connecting the interhemispheric homologous M1, SMA proper, and DLPFC cortices showed significant interaction effects with phase error in different sensory conditions. To further complement these results, we explored the extent to which GM thickness and surface area of these cortical regions predicted phase error. To this end, we identified which cortical subdivisions provided by FreeSurfer (based on the Desikan-Killiany cortical atlas) [Desikan et al., 2006] corresponded to the cortical seed masks used for WM tractography in FSL. Visual inspection revealed that FSL's seed mask of M1 partially overlapped with the 'precentral' region in FreeSurfer, while FSL's mask of SMA proper partially overlapped with the 'paracentral' region in FreeSurfer. FSL's seed mask of DLPFC partially overlapped with both the 'rostral middle frontal' and 'caudal middle frontal' regions in FreeSurfer (Fig. 3b). Therefore, these cortical regions were used for GM analyses to complement the WM results.

Overall, age-related changes in GM with age supported previous literature on brain maturation [Croteau-Chonka et al., 2016; Ducharme et al., 2015, 2016; Gogtay et al., 2004]. More specifically, the thickness of the paracentral and rostral middle frontal cortices decreased with age. Correlations between age and thickness of precentral and caudal middle frontal cortices, and cortical surface of all ROIs, were non-significant (see Supporting Information).

Cortical Surface

Model 3a assessed the extent to which mean cortical surface area predicted phase error, while controlling for total intracranial volume (Table III). Results showed no fixed effects of cortical surface areas on phase error (all

TABLE II. White matter

| | FA | | | | | | MD | | | | | |
| | Model 2a. All ROIs included | | | Model 2b. Sensitivity analysis | | | Model 2c. All ROIs included | | | Model 2d. Sensitivity analysis | | |
Fixed Effects[a]	b	SE	P-value	b	SE	P-value	b	SE	P-value	b	SE	P-value
Intercept	65.020	2.780	<0.001***	65.044	2.634	<0.001***	64.743	2.582	<0.001***	64.596	2.566	<0.001***
Age	−6.005	2.066	0.006**	−6.130	1.984	0.004**	−6.312	1.845	0.001**	−6.804	1.711	<0.001***
Gender	−0.322	3.937	0.935	0.176	3.486	0.960	0.089	3.455	0.979	0.757	3.355	0.823
Trial	−0.525	0.090	<0.001***	−0.557	0.089	<0.001***	−0.517	0.089	<0.001***	−0.538	0.088	<0.001***
Coordination mode In-phase (ref anti-phase)	−1.049	0.786	0.182	−1.051	0.788	0.183	−1.051	0.785	0.181	−1.051	0.788	0.183
Sensory condition VIS + PROP (ref VIS)	−9.821	0.965	<0.001***	−9.803	0.967	<0.001***	−9.828	0.963	<0.001***	−9.814	0.966	<0.001***
Sensory condition PROP (ref VIS)	−8.713	0.963	<0.001***	−8.724	0.965	<0.001***	−8.710	0.962	<0.001***	−8.718	0.965	<0.001***
Sensory condition PROP (ref VIS + PROP)	1.108	0.967	0.252	1.079	0.969	0.266	1.118	0.965	0.247	1.096	0.968	0.258
M1	−1.787	4.135	0.668	−0.0987	2.618	0.708	5.958	5.366	0.272	–	–	–
S1	0.427	2.850	0.881	–	–	–	−5.335	4.468	0.238	–	–	–
SMA proper	−1.171	3.251	0.720	−1.212	2.442	0.622	2.566	2.988	0.395	–	–	–
Pre-SMA	0.723	4.104	0.861	–	–	–	−4.906	3.338	0.148	–	–	–
DLPFC	−0.608	2.499	0.809	–	–	–	1.608	2.658	0.548	1.435	1.781	0.424
M1 × VIS+PROP (ref VIS)	−0.870	2.018	0.666	−1.770	1.324	0.182	−1.406	3.000	0.639	–	–	–
M1 × PROP (ref VIS)	−4.552	2.011	0.024*	−4.181	1.328	0.002 **	−3.011	2.992	0.314	–	–	–
M1 × PROP (ref VIS+PROP)	−3.682	2.015	0.068	−2.411	1.328	0.070	−1.605	2.995	0.592	–	–	–
S1 × VIS+PROP (ref VIS)	1.757	1.514	0.246	–	–	–	2.194	2.499	0.380	–	–	–
S1 × PROP (ref VIS)	2.122	1.512	0.161	–	–	–	3.056	2.495	0.221	–	–	–
S1 × PROP (ref VIS+PROP)	0.365	1.510	0.809	–	–	–	0.862	2.492	0.729	–	–	–
SMA proper × VIS + PROP (ref VIS)	2.354	1.725	0.173	1.626	1.325	0.220	−0.966	1.622	0.551	–	–	–
SMA proper × PROP (ref VIS)	3.504	1.723	0.042*	3.545	1.326	0.008**	−2.594	1.620	0.110	–	–	–
SMA proper × PROP (ref VIS+PROP)	1.151	1.734	0.507	1.918	1.331	0.150	−1.628	1.618	0.315	–	–	–
Pre-SMA × VIS + PROP (ref VIS)	−2.287	2.107	0.278	–	–	–	2.072	1.738	0.234	–	–	–
Pre-SMA × PROP (ref VIS)	−0.560	2.085	0.788	–	–	–	3.066	1.721	0.075	–	–	–
Pre-SMA × PROP (ref VIS+PROP)	1.727	2.112	0.419	–	–	–	0.994	1.732	0.566	–	–	–

TABLE II. (continued).

	FA						MD					
	Model 2a. All ROIs included			Model 2b. Sensitivity analysis			Model 2c. All ROIs included			Model 2d. Sensitivity analysis		
Fixed Effects[a]	b	SE	P-value	b	SE	P-value	b	SE	P-value	b	SE	P-value
DLPFC × VIS+PROP (ref VIS)	−1.516	1.278	0.236	–	–	–	1.138	1.484	0.443	1.968	0.966	0.042*
DLPFC × PROP (ref VIS)	−1.334	1.278	0.297	–	–	–	3.455	1.483	0.020*	3.225	0.965	<0.001***
DLPFC × PROP (ref VIS+PROP)	0.182	1.276	0.887	–	–	–	2.317	1.483	0.119	1.257	0.966	0.193
Random effects	σ^2			σ^2			σ^2			σ^2		
Participants Intercept	105.8			107.9			99.68			103.4		
Residual	148.2			148.9			147.77			148.8		
Effect size (R_c^2)	0.567			0.565			0.569			0.566		

[a]The reference for the fixed effects shown here is, by default, the visual condition. The dependent variable is phase error. Sensory conditions displayed are the VIS, PROP, and VIS + PROP conditions. R_c^2 conditional pseudo R^2. ***$P < 0.001$, **$P < 0.01$, *$P < 0.05$.

$P > 0.05$). However, significant interactions were found between the paracentral cortex (partially overlapping with FSL's mask for SMA proper) and PROP versus VIS ($b = -5.082$, SE = 1.399, $P < 0.001$), and PROP versus VIS + PROP ($b = -3.810$, SE = 1.400, $P = 0.007$). Additionally, interactions between the caudal middle frontal cortex (caudal MFC; partially overlapping with FSL's mask for DLPFC) and PROP versus VIS ($b = 5.514$, SE = 1.329, $P < 0.001$), and PROP versus VIS + PROP ($b = 3.842$, SE = 1.328, $P = 0.004$) were found. To build a more parsimonious model and to confirm the sensitivity of our results, all ROIs identified as non-significant in Model 3a were removed (Model 3b, Table III). This new model predicted the data more accurately than the original model (3a; Δ AIC = −8.4). The interactions between the surface of the paracentral frontal cortex and PROP versus VIS ($b = -4.881$, SE = 1.223, $P < 0.001$) and PROP versus VIS + PROP ($b = -3.550$, SE = 1.222, $P = 0.004$) remained significant, as well as the interactions between the caudal MFC and PROP versus VIS ($b = 5.257$, SE = 1.220, $P < 0.001$), and PROP versus VIS + PROP ($b = 3.948$, SE = 1.219, $P = 0.001$), confirming the robustness of the effects. However, simple slope analyses on the effects of these cortical surfaces on phase error within each sensory condition did not reveal significant effects (all $P > 0.05$; Supporting Information). This suggests that these interactions were not critical to disentangle the sensory-specific effect of surface area on phase error.

Cortical Thickness

Model 3c assessed the extent to which mean cortical thickness predicted phase error, while controlling for total intracranial volume (Table III, Fig. 5b). Results showed a significant fixed effect of the precentral cortex (partially overlapping with FSL's mask for M1; $b = -5.353$, SE = 2.063, $P = 0.013$), with decreasing phase errors from smaller to larger cortical thickness. Additionally, significant interactions were found between the precentral cortex and VIS + PROP versus VIS ($b = 3.563$, SE = 1.277, $P = 0.005$), and PROP versus VIS ($b = 3.131$, SE = 1.255, $P = 0.013$), and between the rostral MFC (partially overlapping with FSL's mask for DLPFC) and VIS + PROP versus VIS ($b = -2.610$, SE = 1.291, $P = 0.043$). To build a more parsimonious model and to confirm the sensitivity of our results, all ROIs identified as non-significant in Model 3c were removed (Model 3d, Table III). This new model predicted the data more accurately than the original model (3c; Δ AIC = −8.2). The fixed effect of the precentral cortex ($b = -7.506$, SE = 1.950, $P < 0.001$) remained significant, as did the interactions between the precentral cortex and VIS + PROP versus VIS ($b = 3.167$, SE = 1.145, $P = 0.006$), and PROP versus VIS ($b = 2.415$, SE = 1.126, $P = 0.032$) (Fig. 5b). Similarly, the interaction between the rostral MFC and VIS + PROP versus VIS remained significant ($b = -2.932$, SE = 1.140, $P = 0.010$) (Supporting Information). This confirms the robustness of the effects. Simple

A. Mean diffusivity

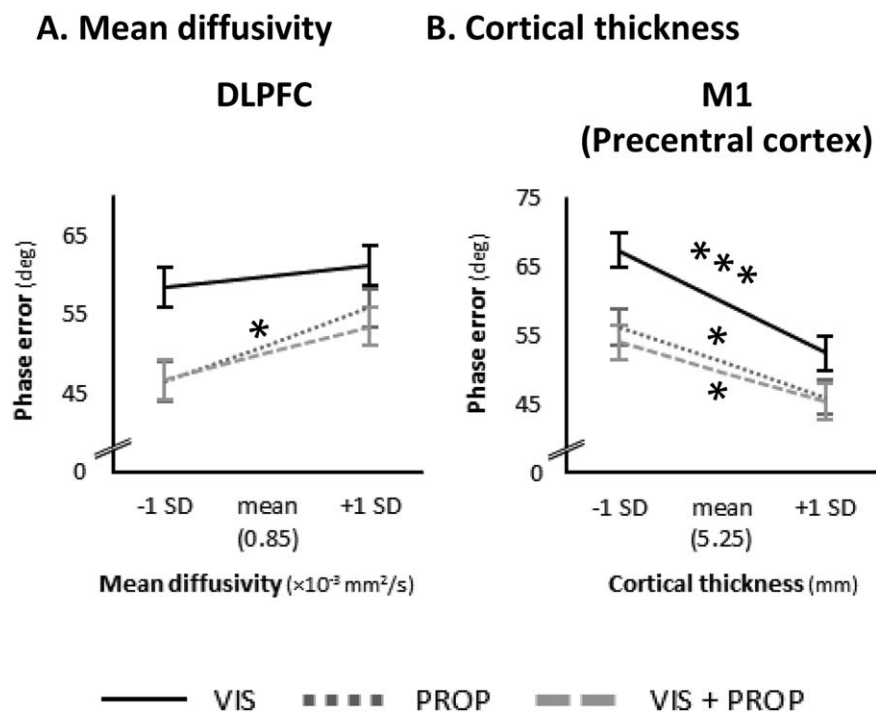## B. Cortical thickness

DLPFC

M1 (Precentral cortex)

Figure 5.

Neural predictors of tracking performance. **(A)** Increasing MD in DLPFC tracts resulted in larger phase errors in PROP ($b = 4.660$), but not in the other sensory conditions. **(B)** Larger cortical thickness of M1 (precentral cortex) resulted in lower phase errors in all sensory conditions. This beneficial effect of M1 cortical thickness was strongest for VIS ($b = -7.506$), compared with PROP ($b = -5.091$) and VIS + PROP ($b = -4.338$). ***$P < 0.001$, *$P < 0.05$.

slope analyses within each sensory condition (VIS + PROP, PROP, VIS) revealed that the beneficial effect of precentral cortical thickness on phase error was strongest in VIS (decreasing phase error; $b = -7.506$, SE = 1.950, $P < 0.001$), and to a lesser extent in PROP ($b = -5.091$, SE = 1.949, $P = 0.012$) and VIS + PROP ($b = -4.338$, SE = 1.956, $P = 0.031$). For simple slope analyses on the effect of rostral MFC thickness on phase error within each condition (VIS + PROP, VIS), no significant effects were found (all $P > 0.05$; Supporting Information). This suggests that these latter interactions between rostral MFC thickness and VIS + PROP versus VIS were not critical to disentangle the sensory-specific effect of FA on phase error.

DISCUSSION

In this study, we investigated the relative contribution of visual and proprioceptive information to performance on a manual tracking task and the extent to which structural brain measures predict this performance in participants aged 9–18 years. Results showed that tracking performance was poorer when visual information was available (not related to own movement), compared with proprioceptive or combined sensory information (related

to own movement). Additionally, the microstructural organization of WM connections between the interhemispheric homologous DLPFC and cortical thickness of M1 (i.e., precentral cortex) were associated with sensory-specific tracking performance.

Tracking Performance and the Role of Sensory Information

On a behavioral level, our results showed that in-phase movements were performed with higher accuracy than anti-phase movements, particularly in younger participants. As the accurate tracking of the passive limb movement resulted from continuous comparison of sensory information from both limbs, the sensory processes involved in our bimanual tracking task were to some extent similar to the ones involved in active bimanual coordination tasks. Results on bimanual coordination skills in children, showing better performance during in-phase as compared with anti-phase coordination, are consistent with those observed in the present study, supporting this converging perspective [Salter et al., 2004]. Additionally, it has been reported that younger children are less proficient with anti-phase coordination than adults, which is possibly due to a reduced ability to inhibit or suppress

TABLE III. Gray matter

	Cortical Surface						Cortical Thickness					
	Model 3a. All ROIs included			Model 3b. Sensitivity analysis			Model 3c. All ROIs included			Model 3d. Sensitivity analysis		
Fixed effects[a]	b	SE	P-value	b	SE	P-value	b	SE	P-value	b	SE	P-value
Intercept	65.909	3.038	<0.001***	66.113	2.989	<0.001***	65.082	2.782	< 0.001 ***	65.803	2.673	< 0.001 ***
Age	−7.786	1.860	< 0.001 ***	−7.943	1.857	<0.001***	−6.350	2.502	0.015 *	−7.313	2.080	0.001 **
Gender	−1.542	4.564	0.737	−1.922	4.394	0.664	0.058	4.176	0.989	−1.708	3.801	0.656
Trial	−0.540	0.088	< 0.001***	−0.542	0.088	<0.001***	−0.530	0.092	< 0.001***	−0.515	0.091	<0.001***
Coordination mode in-phase (ref anti-phase)	−1.292	0.788	0.101	−1.292	0.789	0.102	−1.299	0.793	0.102	−1.296	0.795	0.103
Sensory condition VIS +PROP (ref VIS)	−10.219	0.966	< 0.001***	−10.216	0.967	< 0.001***	−10.236	0.973	< 0.001***	−10.243	0.975	<0.001***
Sensory condition PROP (ref VIS)	−8.820	0.964	< 0.001***	−8.820	0.966	< 0.001***	−8.818	0.971	< 0.001***	−8.815	0.973	<0.001***
Sensory condition PROP (ref VIS + PROP)	1.399	0.967	0.148	1.396	0.969	0.150	1.418	0.974	0.146	1.428	0.976	0.144
Total intracranial volume	−4.142	2.353	0.086	−3.873	2.363	0.109	−3.244	1.853	0.088	−3.228	1.878	0.094
Precentral frontal cortex	3.825	2.813	0.181	–	–	–	−7.568	2.186	0.001**	−7.506	1.950	<0.001***
Paracentral frontal cortex	3.601	2.807	0.206	3.514	2.579	0.180	1.489	2.818	0.600	–	–	–
Rostral middle frontal cortex	−2.329	3.197	0.470	–	–	–	4.842	2.602	0.069	4.147	2.423	0.094
Caudal middle frontal cortex	−3.075	2.550	0.234	−2.469	2.404	0.310	−1.279	2.572	0.621	–	–	–
Precentral frontal cortex × VIS+PROP (ref VIS)	−1.786	1.462	0.222	–	–	–	3.563	1.277	0.005**	3.167	1.145	0.006**
Precentral frontal cortex × PROP (ref VIS)	−2.136	1.456	0.143	–	–	–	3.131	1.255	0.013*	2.415	1.126	0.032*
Precentral frontal cortex × PROP (ref VIS+PROP)	−0.350	1.462	0.811	–	–	–	−0.432	1.277	0.735	−0.752	1.135	0.508
Paracentral frontal cortex × VIS+PROP (ref VIS)	−1.273	1.399	0.363	−1.330	1.221	0.276	0.282	1.269	0.824	–	–	–
Paracentral frontal cortex × PROP (ref VIS)	−5.082	1.399	< 0.001***	−4.881	1.223	<0.001***	0.876	1.270	0.491	–	–	–
Paracentral frontal cortex × PROP (ref VIS+PROP)	−3.810	1.400	0.007**	−3.550	1.222	0.004**	0.594	1.273	0.641	–	–	–
Rostral middle frontal cortex × VIS+PROP (ref VIS)	1.022	1.656	0.537	–	–	–	−2.610	1.291	0.043*	−2.932	1.140	0.010*
Rostral middle frontal cortex × PROP (ref VIS)	1.779	1.653	0.282	–	–	–	−1.327	1.312	0.312	−1.787	1.143	0.118
Rostral middle frontal cortex × PROP (ref VIS+PROP)	0.756	1.657	0.648	–	–	–	1.283	1.282	0.317	1.145	1.128	0.310

TABLE III. (continued).

Fixed effects[a]	Cortical Surface						Cortical Thickness					
	Model 3a. Al ROIs included			Model 3b. Sensitivity analysis			Model 3c. All ROIs included			Model 3d. Sensitivity analysis		
	b	SE	P-value	b	SE	P-value	b	SE	P-value	b	SE	P-value
Caudal middle frontal cortex × VIS+PROP (ref VIS)	1.672	1.329	0.208	1.309	1.219	0.283	−1.182	1.370	0.389	–	–	–
Caudal middle frontal cortex × PROP (ref VIS)	5.514	1.329	< 0.001***	5.257	1.219	< 0.001***	−2.270	1.376	0.099	–	–	–
Caudal middle frontal cortex × PROP (ref VIS+PROP)	3.842	1.328	0.004**	3.948	1.219	0.001**	−1.088	1.371	0.427	–	–	–
Random effects	σ^2			σ^2			σ^2			σ^2		
Participants Intercept	107.50			110.2			84.89			87.34		
Residual	141.20			141.7			143.29			143.75		
Effect size (R_c^2)	0.591			0.590			0.584			0.583		

[a]The reference for the fixed effects shown here is, by default, the visual condition. The dependent variable is phase error. Sensory conditions displayed are the VIS, PROP, and VIS + PROP conditions. R_c^2 conditional pseudo R^2. ***$P < 0.001$, **$P < 0.01$, *$P < 0.05$.

unwanted (mirror) movements [De Boer et al., 2012]. Furthermore, our results showed that the older cohort of participants performed better than the younger participants during both in-phase and anti-phase coordination, confirming earlier results on general age-related improvements in joint position matching tasks [Bremner et al., 2013; Contreras-Vidal, 2006; Goble et al., 2005; Van Roon et al., 2008].

Considering sensory contributions to tracking accuracy, we found that overall tracking accuracy across the age span was better when proprioceptive information was available. Using a similar paradigm as ours in young adults, a proprioceptive advantage was also reported, albeit specifically during in-phase coordination [Alaerts et al., 2007]. During anti-phase coordination, a visual advantage was reported. Alaerts and coworkers suggested that young adults were able to up-weight internal feedback proprioception over external feedback vision during in-phase coordination, to monitor the synchrony of homologous muscle activations [Carson et al., 1995; Kelso, 1984; Salter et al., 2004; Swinnen et al., 1998; Temprado et al., 2003]. Conversely, external feedback was up-weighted during anti-phase coordination to detect the spatial convergence of the external stimuli, that is, the iso-directional (parallel) motions of the limbs in extrinsic space [Alaerts et al., 2007; Bogaerts et al., 2003; Mechsner et al., 2001]. However, this account may be less useful for our results. In our visual tracking condition, the active limb was covered by an opaque box. Therefore, this condition tested the ability to integrate visual and proprioceptive information. Contrasting with Alaerts et al. [2007], our visual condition prevented direct between-limb comparison of visual information (central or peripheral). Conditions with available proprioceptive information were the only ones in which information of both limbs was provided by the same sensory system. As the brain has been shown to give priority to sensory inputs available bilaterally over the ones available in a single limb only [Boisgontier and Nougier, 2013], this may explain why our results showed a proprioceptive advantage in both in-phase and anti-phase tracking, while Alaerts et al. [2007] revealed a more coordination mode-specific contribution of sensory feedback.

Although speculative, another explanation for the proprioceptive advantage found in our tracking task, might be related to hand preference and hemispheric specialization. In our task, tracking movements were performed with the left (non-preferred) hand. Earlier studies on bimanual matching in adults have indicated sensory-specific matching performance when either the preferred or non-preferred hand was used [Goble et al., 2006; Goble and Brown, 2008]. The non-preferred hand relied more on proprioceptive feedback, while the preferred hand relied more on visual feedback. It was suggested that this was due to hemispheric specialization in sensory processing. More specifically, the dominance of the right hemisphere for proprioceptive processing allowed the contralateral

(left) hand preferential access to this information [Goble and Brown, 2008; Haaland et al., 2004]. In our study, the proprioceptive advantage may thus be caused by favoring proprioceptive over visual information for non-dominant limb performance. Although we did not investigate hemispheric asymmetry in our study, we must be aware of the possibility that this process may have influenced our results. However, future studies are needed to establish a direct causal link to support this argumentation.

Structural Brain Predictors of Tracking Performance in Youth

Using CSD, a state-of-the-art WM tractography method alleviating the crossing fibers problem, we were able to investigate the microstructural properties of several WM tracts connecting homologous key brain regions involved in manual motor control. Although our results did not show fixed effects of microstructural organization on overall tracking performance, interactions between sensory conditions did suggest sensory-specific relations between microstructure of DLPFC WM tracts and tracking performance. In particular during proprioceptive tracking, the beneficial relation between increased microstructural organization (i.e., lower MD) of DLPFC tracts and performance accuracy (lower phase error) was present, but not in visual or combined visual and proprioceptive tracking. The DLPFC has previously been related to cognitive control over action, referring to proper deployment of attention to action and use of working memory to meet the goal of the task [Beets et al., 2015; Cieslik et al., 2013; Fujiyama et al., 2016; Fuster, 2001; Hoshi, 2006; Lucci et al., 2014; Miller and Cohen, 2001; Pochon et al., 2001; Remy et al., 2008]. Therefore, we suggest that proprioceptive tracking demands a high working memory load and to pay attention to the sensory information of the target limb, temporarily store it in memory, and translate this into appropriate movement of the contralateral limb. The contribution of the DLPFC to proprioceptive tracking performance has already been shown using tendon vibration paradigms [Goble et al., 2012a] and may possibly be related to the generally accepted concept that passive movements provide lower proprioceptive acuity than active movements [Craske and Crawshaw, 1975; Gritsenko et al., 2007; Laufer et al., 2001; but see Capaday et al., 2013]. Passive movements lack information from internal forward models which estimate limb position based on the motor command and the neuromuscular information of the limb during the movement. In our study, the proprioceptive acuity of the passively moved target limb may thus have been compromised, and this could have been compensated by placing a higher load on prefrontal processes such as attention and working memory. This theory is supported by results obtained by Boisgontier et al. [2014] using a similar task setup. They revealed that tracking performance improved when overt attention was directed towards the passively moving target limb, while redirecting attention away from the target limb (i.e., towards the active limb) impaired tracking performance. Interestingly, matching tasks are often used to measure proprioceptive acuity and are thought to rely primarily on sensorimotor processes [Gomez-Moya et al., 2016; King et al., 2010]. However, our current result also suggests an important contribution of interhemispheric WM connections between DLPFC regions. Although the GM results did not backup these findings, it is reasonable to suggest that tracking tasks benefit from efficient neural pathways that facilitate deployment of attention and working memory. This may also imply that participants performing these tasks with lower accuracy may have a deficit in working memory and attention, as also appears to be the case in older adults [Boisgontier et al., 2012; Goble et al., 2012b].

Furthermore, GM analyses showed that a larger cortical thickness of M1 was related to higher performance accuracy (lower phase error) in all sensory conditions, with the strongest effect obtained in visual tracking. These findings are consistent with previous literature, showing that M1 is functionally associated with movement planning and execution [Gao et al., 2014; Gentilucci et al., 2000; Immisch et al., 2001; Jancke et al., 2000; Swinnen and Wenderoth, 2004; Toyokura et al., 1999, 2002], and larger thickness of motor regions relates to improved performance on motor tasks [Anderson et al., 2002]. Our results add to this existing knowledge by showing that the strength of the association between M1 thickness and tracking accuracy of passive movements depends on the available sensory information. Particularly for visually guided movements, the beneficial effect of larger M1 thickness was stronger, compared with the other sensory conditions (PROP and VIS + PROP). In our study, the visual condition provided mainly external movement triggers, while the proprioceptive condition and the combined sensory information condition were guided by internal triggers afforded by the proprioceptive system. It has been suggested that functional coupling between motor regions (e.g., M1 and SMA) is generally stronger during internally versus externally triggered movements [Gerloff et al., 1998; Myers and Mackinnon, 2004], and the SMA is particularly associated with internally triggered rather than externally triggered movements [Debaere et al., 2003; Deiber et al., 1999; Goldberg, 1985; Jenkins et al., 2000; Nachev et al., 2005, 2008]. Following these suggestions, we tentatively propose that tracking accuracy of internally triggered movements (PROP and VIS + PROP) depends on an interplay between several motor regions (e.g., SMA and M1), whereas the tracking accuracy of externally triggered movements (VIS) are particularly represented by M1 functionality.

In conclusion, tracking accuracy in youth was differently associated with microstructural organization of the DLPFC tracts and cortical thickness of M1, depending on available sensory information. These results suggest that joint

position matching tasks, which are often used to measure proprioceptive acuity, do not only rely on sensorimotor processing regions but also on prefrontal regions involved in attention and working memory. This implies that participants who exhibit deficits in working memory and attention may also be less accurate during these sensory-driven matching tasks.

ACKNOWLEDGMENTS

REFERENCES

Alaerts K, Levin O, Swinnen SP (2007): Whether feeling or seeing is more accurate depends on tracking direction within the perception-action cycle. Behav Brain Res 178:229–234.

Anderson BJ, Eckburg PB, Relucio KI (2002): Alterations in the thickness of motor cortical subregions after motor-skill learning and exercise. Learn Mem 9:1–9.

Basser PJ (1997): New histological and physiological stains derived from diffusion-tensor MR images. Ann N Y Acad Sci 820:123–138.

Basser PJ, Jones DK (2002): Diffusion-tensor MRI: theory, experimental design and data analysis - a technical review. NMR Biomed 15:456–467.

Basser PJ, Mattiello J, LeBihan D (1994): Estimation of the effective self-diffusion tensor from the NMR spin echo. J Magn Reson B 103:247–254.

Basser PJ, Pierpaoli C (1996): Microstructural and physiological features of tissues elucidated by quantitative-diffusion-tensor MRI. J Magn Reson B 111:209–219.

Beaulieu C (2002): The basis of anisotropic water diffusion in the nervous system - a technical review. NMR Biomed 15:435–455.

Beaulieu C, Allen PS (1994): Determinants of anisotropic water diffusion in nerves. Magn Reson Med 31:394–400.

Beets IA, Gooijers J, Boisgontier MP, Pauwels L, Coxon JP, Wittenberg G, Swinnen SP (2015): Reduced neural differentiation between feedback conditions after bimanual coordination training with and without augmented visual feedback. Cereb Cortex 25:1958–1969.

Birtles D, Anker S, Atkinson J, Shellens R, Briscoe A, Mahoney M, Braddick O (2011): Bimanual strategies for object retrieval in infants and young children. Exp Brain Res 211:207–218.

Boashash B (1992a): Estimating and interpreting the instantaneous frequency of a signal. 1. Fundamentals. Proc IEEE Inst Electr Electron Eng 80:520–538.

Boashash B (1992b): Estimating and interpreting the instantaneous frequency of a signal. 2. Algorithms and applications. Proc IEEE Inst Electr Electron Eng 80:540–568.

Bogaerts H, Buekers MJ, Zaal FT, Swinnen SP (2003): When visuomotor incongruence aids motor performance: the effect of perceiving motion structures during transformed visual feedback on bimanual coordination. Behav Brain Res 138:45–57.

Boisgontier MP, Cheval B (2016): The anova to mixed model transition. Neurosci Biobehav Rev 68:1004–1005.

Boisgontier MP, Nougier V (2013): Proprioception: bilateral inputs first. Neurosci Lett 534:96–100.

Boisgontier MP, Olivier I, Chenu O, Nougier V (2012): Presbypropria: the effects of physiological ageing on proprioceptive control. Age (Dordr) 34:1179–1194.

Boisgontier MP, Van Halewyck F, Corporaal SH, Willacker L, Van Den Bergh V, Beets IA, Levin O, Swinnen SP (2014): Vision of the active limb impairs bimanual motor tracking in young and older adults. Front Aging Neurosci 6:320.

Bremner AJ, Hill EL, Pratt M, Rigato S, Spence C (2013): Bodily illusions in young children: developmental change in visual and proprioceptive contributions to perceived hand position. PLoS One 8:e51887.

Capaday C, Darling WG, Stanek K, Van Vreeswijk C (2013): Pointing to oneself: active versus passive proprioception revisited and implications for internal models of motor system function. Exp Brain Res 229:171–180.

Carson RG, Goodman D, Kelso JA, Elliott D (1995): Phase transitions and critical fluctuations in rhythmic coordination of ipsilateral hand and foot. J Mot Behav 27:211–224.

Carson RG, Smethurst CJ, Forner M, Meichenbaum DP, Mackey DC (2002): Role of peripheral afference during acquisition of a complex coordination task. Exp Brain Res 144:496–505.

Chai T, Draxler RR (2014): Root mean square error (RMSE) or mean absolute error (MAE)? - Arguments against avoiding RMSE in the literature. Geosci Model Dev 7:1247–1250.

Cieslik EC, Zilles K, Caspers S, Roski C, Kellermann TS, Jakobs O, Langner R, Laird AR, Fox PT, Eickhoff SB (2013): Is there "one" DLPFC in cognitive action control? Evidence for heterogeneity from co-activation-based parcellation. Cereb Cortex 23:2677–2689.

Contreras-Vidal JL (2006): Development of forward models for hand localization and movement control in 6-to 10-year-old children. Hum Mov Sci 25:634–645.

Craske B, Crawshaw M (1975): Shifts in kinesthesis through time and after active and passive movement. Percept Mot Skills 40:755–761.

Croteau-Chonka EC, Dean DC, 3rd, Remer J, Dirks H, O'Muircheartaigh J, Deoni SC (2016): Examining the relationships between cortical maturation and white matter myelination throughout early childhood. Neuroimage 125:413–421.

Dale AM, Fischl B, Sereno MI (1999): Cortical surface-based analysis - I. Segmentation and surface reconstruction. Neuroimage 9:179–194.

Dale AM, Sereno MI (1993): Improved localization of cortical activity by combining eeg and meg with mri cortical surface reconstruction - a linear-approach. J Cogn Neurosci 5:162–176.

De Boer BJ, Peper CE, Beek PJ (2012): Development of temporal and spatial bimanual coordination during childhood. Motor Control 16:537–559.

Debaere F, Wenderoth N, Sunaert S, Van Hecke P, Swinnen SP (2003): Internal vs external generation of movements: differential neural pathways involved in bimanual coordination performed in the presence or absence of augmented visual feedback. Neuroimage 19:764–776.

Debaere F, Wenderoth N, Sunaert S, Van Hecke P, Swinnen SP (2004): Cerebellar and premotor function in bimanual coordination: parametric neural responses to spatiotemporal complexity and cycling frequency. Neuroimage 21:1416–1427.

Deiber MP, Honda M, Ibanez V, Sadato N, Hallett M (1999): Mesial motor areas in self-initiated versus externally triggered

movements examined with fMRI: effect of movement type and rate. J Neurophysiol 81:3065–3077.

Desikan RS, Segonne F, Fischl B, Quinn BT, Dickerson BC, Blacker D, Buckner RL, Dale AM, Maguire RP, Hyman BT, Albert MS, Killiany RJ (2006): An automated labeling system for subdividing the human cerebral cortex on MRI scans into gyral based regions of interest. Neuroimage 31:968–980.

Ducharme S, Albaugh MD, Nguyen TV, Hudziak JJ, Mateos-Perez JM, Labbe A, Evans AC, Karama S (2015): Trajectories of cortical surface area and cortical volume maturation in normal brain development. Data Brief 5:929–938.

Ducharme S, Albaugh MD, Nguyen TV, Hudziak JJ, Mateos-Perez JM, Labbe A, Evans AC, Karama S (2016): Trajectories of cortical thickness maturation in normal brain development - The importance of quality control procedures. Neuroimage 125: 267–279.

Emsell, L, Van Hecke, W, Tournier, JD (2016): Introduction to diffusion tensor imaging. In: Van Hecke, W, Emsell, L, Sunaert, S, editors. Diffusion Tensor Imaging. New York: Springer. pp 7–19.

Fischl B, Dale AM (2000): Measuring the thickness of the human cerebral cortex from magnetic resonance images. Proc Natl Acad Sci U S A 97:11050–11055.

Fischl B, Salat DH, Busa E, Albert M, Dieterich M, Haselgrove C, van der Kouwe A, Killiany R, Kennedy D, Klaveness S, Montillo A, Makris N, Rosen B, Dale AM (2002): Whole brain segmentation: automated labeling of neuroanatomical structures in the human brain. Neuron 33:341–355.

Fischl B, Salat DH, van der Kouwe AJW, Makris N, Segonne F, Quinn BT, Dale AM (2004a): Sequence-independent segmentation of magnetic resonance images. Neuroimage 23:S69–S84.

Fischl B, van der Kouwe A, Destrieux C, Halgren E, Segonne F, Salat DH, Busa E, Seidman LJ, Goldstein J, Kennedy D, Caviness V, Makris N, Rosen B, Dale AM (2004b): Automatically parcellating the human cerebral cortex. Cereb Cortex 14: 11–22.

Frazier JA, Chiu SF, Breeze JL, Makris N, Lange N, Kennedy DN, Herbert MR, Bent EK, Koneru VK, Dieterich ME, Hodge SM, Rauch SL, Grant PE, Cohen BM, Seidman LJ, Caviness VS, Biederman J (2005): Structural brain magnetic resonance imaging of limbic and thalamic volumes in pediatric bipolar disorder. Am J Psychiatry 162:1256–1265.

Fujiyama H, Van Soom J, Rens G, Gooijers J, Leunissen I, Levin O, Swinnen SP (2016): Age-related changes in frontal network structural and functional connectivity in relation to bimanual movement control. J Neurosci 36:1808–1822.

Fuster JM (2001): The prefrontal cortex–an update: time is of the essence. Neuron 30:319–333.

Gao Q, Tao Z, Zhang M, Chen H (2014): Differential contribution of bilateral supplementary motor area to the effective connectivity networks induced by task conditions using dynamic causal modeling. Brain Connect 4:256–264.

Gautam P, Anstey KJ, Wen W, Sachdev PS, Cherbuin N (2015): Cortical gyrification and its relationships with cortical volume, cortical thickness, and cognitive performance in healthy midlife adults. Behav Brain Res 287:331–339.

Gentilucci M, Bertolani L, Benuzzi F, Negrotti A, Pavesi G, Gangitano M (2000): Impaired control of an action after supplementary motor area lesion: a case study. Neuropsychologia 38:1398–1404.

Gerloff C, Richard J, Hadley J, Schulman AE, Honda M, Hallett M (1998): Functional coupling and regional activation of human

cortical motor areas during simple, internally paced and externally paced finger movements. Brain 121: 1513–1531.

Geyer S, Schormann T, Mohlerg H, Zilles K (2000): Areas 3a, 3b, and 1 of human primary somatosensory cortex: 2. Spatial normalization to standard anatomical space. Neuroimage 11:684–696.

Goble DJ, Brown SH (2008): Upper limb asymmetries in the matching of proprioceptive versus visual targets. J Neurophysiol 99: 3063–3074.

Goble DJ, Coxon JP, Van Impe A, Geurts M, Van Hecke W, Sunaert S, Wenderoth N, Swinnen SP (2012a): The neural basis of central proprioceptive processing in older versus younger adults: an important sensory role for right putamen. Hum Brain Mapp 33:895–908.

Goble DJ, Lewis CA, Brown SH (2006): Upper limb asymmetries in the utilization of proprioceptive feedback. Exp Brain Res 168: 307–311.

Goble DJ, Lewis CA, Hurvitz EA, Brown SH (2005): Development of upper limb proprioceptive accuracy in children and adolescents. Hum Mov Sci 24:155–170.

Goble DJ, Mousigian MA, Brown SH (2012b): Compromised encoding of proprioceptively determined joint angles in older adults: the role of working memory and attentional load. Exp Brain Res 216:35–40.

Gogtay N, Giedd JN, Lusk L, Hayashi KM, Greenstein D, Vaituzis AC, Nugent TF, 3rd, Herman DH, Clasen LS, Toga AW, Rapoport JL, Thompson PM (2004): Dynamic mapping of human cortical development during childhood through early adulthood. Proc Natl Acad Sci U S A 101: 8174–8179.

Goldberg G (1985): Supplementary motor area structure and function - review and hypotheses. Behav Brain Sci 8:567–588.

Goldstein JM, Seidman LJ, Makris N, Ahern T, O'Brien LM, Caviness VS, Kennedy DN, Faraone SV, Tsuang MT (2007): Hypothalamic abnormalities in schizophrenia: Sex effects and genetic vulnerability. Biol Psychiatry 61:935–945.

Gomez-Moya R, Diaz R, Fernandez-Ruiz J (2016): Different visuomotor processes maturation rates in children support dual visuomotor learning systems. Hum Mov Sci 46: 221–228.

Gooijers J, Swinnen SP (2014): Interactions between brain structure and behavior: The corpus callosum and bimanual coordination. Neurosci Biobehav Rev 43:1–19.

Grefkes C, Eickhoff SB, Nowak DA, Dafotakis M, Fink GR (2008): Dynamic intra- and interhemispheric interactions during unilateral and bilateral hand movements assessed with fMRI and DCM. Neuroimage 41:1382–1394.

Grefkes C, Geyer S, Schormann T, Roland P, Zilles K (2001): Human somatosensory area 2: Observer-independent cytoarchitectonic mapping, interindividual variability, and population map. Neuroimage 14:617–631.

Gritsenko V, Krouchev NI, Kalaska JF (2007): Afferent input, efference copy, signal noise, and biases in perception of joint angle during active versus passive elbow movements. J Neurophysiol 98:1140–1154.

Haaland KY, Prestopnik JL, Knight RT, Lee RR (2004): Hemispheric asymmetries for kinematic and positional aspects of reaching. Brain 127:1145–1158.

Hair., JF, Anderson, RE, Tatham, RL, Black, WC (1995): Multivariate Data Analysis. 3rd ed. New York: Macmillan.

Haring L, Muursepp A, Mottus R, Ilves P, Koch K, Uppin K, Tarnovskaja J, Maron E, Zharkovsky A, Vasar E, Vasar V (2016): Cortical thickness and surface area correlates with

cognitive dysfunction among first-episode psychosis patients. Psychol Med 46:2145–2155.

Hoshi E (2006): Functional specialization within the dorsolateral prefrontal cortex: a review of anatomical and physiological studies of non-human primates. Neurosci Res 54:73–84.

Immisch I, Waldvogel D, van Gelderen P, Hallett M (2001): The role of the medial wall and its anatomical variations for bimanual antiphase and in-phase movements. Neuroimage 14: 674–684.

Jancke L, Peters M, Himmelbach M, Nosselt T, Shah J, Steinmetz H (2000): fMRI study of bimanual coordination. Neuropsychologia 38:164–174.

Jarbo K, Verstynen T, Schneider W (2012): In vivo quantification of global connectivity in the human corpus callosum. Neuroimage 59:1988–1996.

Jenkins IH, Jahanshahi M, Jueptner M, Passingham RE, Brooks DJ (2000): Self-initiated versus externally triggered movements. II. The effect of movement predictability on regional cerebral blood flow. Brain 123: 1216–1228.

Kagerer FA, Clark JE (2014): Development of interactions between sensorimotor representations in school-aged children. Hum Mov Sci 34:164–177.

Kelso JA (1984): Phase transitions and critical behavior in human bimanual coordination. Am J Physiol 246:R1000–R1004.

King BR, Pangelinan MM, Kagerer FA, Clark JE (2010): Improvements in proprioceptive functioning influence multisensory-motor integration in 7- to 13-year-old children. Neurosci Lett 483:36–40.

Koeneke S, Lutz K, Wustenberg T, Jancke L (2004): Bimanual versus unimanual coordination: what makes the difference?. Neuroimage 22:1336–1350.

Langevin LM, MacMaster FP, Dewey D (2015): Distinct patterns of cortical thinning in concurrent motor and attention disorders. Dev Med Child Neurol 57:257–264.

Laufer Y, Hocherman S, Dickstein R (2001): Accuracy of reproducing hand position when using active compared with passive movement. Physiother Res Int 6:65–75.

Le Bihan D (1995): Diffusion, perfusion and functional magnetic resonance imaging. J Mal Vasc 20:203–214.

Leemans, A, Jeurissen, B, Sijbers, J, Jones, DK. (2009) ExploreDTI: a graphical toolbox for processing, analyzing, and visualizing diffusion MR data. 17th Annual Meeing of Intl Soc Mag Reson Med. Hawaii, USA. pp 35–37.

Liu J, Morel A, Wannier T, Rouiller EM (2002): Origins of callosal projections to the supplementary motor area (SMA): a direct comparison between pre-SMA and SMA-proper in macaque monkeys. J Comp Neurol 443:71–85.

Lucci G, Berchicci M, Spinelli D, Di Russo F (2014): The motor preparation of directionally incompatible movements. Neuroimage 91:33–42.

Makris N, Goldstein JM, Kennedy D, Hodge SM, Caviness VS, Faraone SV, Tsuang MT, Seidman LJ (2006): Decreased volume of left and total anterior insular lobule in schizophrenia. Schizophr Res 83:155–171.

Mayka MA, Corcos DM, Leurgans SE, Vaillancourt DE (2006): Three-dimensional locations and boundaries of motor and pre-motor cortices as defined by functional brain imaging: A meta-analysis. Neuroimage 31:1453–1474.

Mechsner F, Kerzel D, Knoblich G, Prinz W (2001): Perceptual basis of bimanual coordination. Nature 414:69–73.

Miller EK, Cohen JD (2001): An integrative theory of prefrontal cortex function. Annu Rev Neurosci 24:167–202.

Myers LJ, Mackinnon CD (2004): The time course of functional coupling between human cortical motor areas during internally driven vs. externally cued movements. Conf Proc IEEE Eng Med Biol Soc 6:4669–4672.

Nachev P, Kennard C, Husain M (2008): Functional role of the supplementary and pre-supplementary motor areas. Nat Rev Neurosci 9:856–869.

Nachev P, Rees G, Parton A, Kennard C, Husain M (2005): Volition and conflict in human medial frontal cortex. Curr Biol 15: 122–128.

Naito E (2004): Sensing limb movements in the motor cortex: how humans sense limb movement. Neuroscientist 10:73–82.

Oldfield RC (1971): The assessment and analysis of handedness: the Edinburgh inventory. Neuropsychologia 9:97–113.

Panizzon MS, Fennema-Notestine C, Eyler LT, Jernigan TL, Prom-Wormley E, Neale M, Jacobson K, Lyons MJ, Grant MD, Franz CE, Xian H, Tsuang M, Fischl B, Seidman L, Dale A, Kremen WS (2009): Distinct genetic influences on cortical surface area and cortical thickness. Cereb Cortex 19:2728–2735.

Pochon JB, Levy R, Poline JB, Crozier S, Lehericy S, Pillon B, Deweer B, Le Bihan D, Dubois B (2001): The role of dorsolateral prefrontal cortex in the preparation of forthcoming actions: an fMRI study. Cereb Cortex 11:260–266.

Rakic P (1988): Specification of cerebral cortical areas. Science 241: 170–176.

Rakic P (2007): The radial edifice of cortical architecture: from neuronal silhouettes to genetic engineering. Brain Res Rev 55: 204–219.

Remy F, Wenderoth N, Lipkens K, Swinnen SP (2008): Acquisition of a new bimanual coordination pattern modulates the cerebral activations elicited by an intrinsic pattern: an fMRI study. Cortex 44:482–493.

Reuter M, Rosas HD, Fischl B (2010): Highly accurate inverse consistent registration: a robust approach. Neuroimage 53: 1181–1196.

Salter JE, Wishart LR, Lee TD, Simon D (2004): Perceptual and motor contributions to bimanual coordination. Neurosci Lett 363:102–107.

Salthouse TA, Habeck C, Razlighi Q, Barulli D, Gazes Y, Stern Y (2015): Breadth and age-dependency of relations between cortical thickness and cognition. Neurobiol Aging 36:3020–3028.

Shaw P, Lerch J, Greenstein D, Sharp W, Clasen L, Evans A, Giedd J, Castellanos FX, Rapoport J (2006): Longitudinal mapping of cortical thickness and clinical outcome in children and adolescents with attention-deficit/hyperactivity disorder. Arch Gen Psychiatry 63:540–549.

Sled JG, Zijdenbos AP, Evans AC (1998): A nonparametric method for automatic correction of intensity nonuniformity in MRI data. IEEE Trans Med Imaging 17:87–97.

Smith PF (2012): A note on the advantages of using linear mixed model analysis with maximal likelihood estimation over repeated measures ANOVAs in psychopharmacology: comment on Clark et al. (2012). J Psychopharmacol 26:1605–1607.

Smith SM (2002): Fast robust automated brain extraction. Hum Brain Mapp 17:143–155.

Smith SM, Jenkinson M, Johansen-Berg H, Rueckert D, Nichols TE, Mackay CE, Watkins KE, Ciccarelli O, Cader MZ, Matthews PM, Behrens TEJ (2006): Tract-based spatial statistics: Voxelwise analysis of multi-subject diffusion data. Neuroimage 31:1487–1505.

Smith SM, Jenkinson M, Woolrich MW, Beckmann CF, Behrens TEJ, Johansen-Berg H, Bannister PR, De Luca M, Drobnjak I,

Flitney DE, Niazy RK, Saunders J, Vickers J, Zhang YY, De Stefano N, Brady JM, Matthews PM (2004): Advances in functional and structural MR image analysis and implementation as FSL. Neuroimage 23:S208–S219.

Swinnen SP, Jardin K, Verschueren S, Meulenbroek R, Franz L, Dounskaia N, Walter CB (1998): Exploring interlimb constraints during bimanual graphic performance: effects of muscle grouping and direction. Behav Brain Res 90:79–87.

Swinnen SP, Wenderoth N (2004): Two hands, one brain: cognitive neuroscience of bimanual skill. Trends Cogn Sci 8: 18–25.

Temprado JJ, Swinnen SP, Carson RG, Tourment A, Laurent M (2003): Interaction of directional, neuromuscular and egocentric constraints on the stability of preferred bimanual coordination patterns. Hum Mov Sci 22:339–363.

Tournier JD, Calamante F, Connelly A (2007): Robust determination of the fibre orientation distribution in diffusion MRI: Nonnegativity constrained super-resolved spherical deconvolution. Neuroimage 35:1459–1472.

Tournier JD, Calamante F, Connelly A (2012): MRtrix: Diffusion tractography in crossing fiber regions. Int J Imaging Syst Technol 22:53–66.

Tournier JD, Calamante F, Gadian DG, Connelly A (2004): Direct estimation of the fiber orientation density function from diffusion-weighted MRI data using spherical deconvolution. Neuroimage 23:1176–1185.

Tournier JD, Mori S, Leemans A (2011): Diffusion tensor imaging and beyond. Magn Reson Med 65:1532–1556.

Tournier JD, Yeh CH, Calamante F, Cho KH, Connelly A, Lin CP (2008): Resolving crossing fibres using constrained spherical deconvolution: Validation using diffusion-weighted imaging phantom data. Neuroimage 42:617–625.

Toyokura M, Muro I, Komiya T, Obara M (1999): Relation of bimanual coordination to activation in the sensorimotor cortex and supplementary motor area: analysis using functional magnetic resonance imaging. Brain Res Bull 48:211–217.

Toyokura M, Muro I, Komiya T, Obara M (2002): Activation of pre-supplementary motor area (SMA) and SMA proper during unimanual and bimanual complex sequences: an analysis using functional magnetic resonance imaging. J Neuroimaging 12:172–178.

Tuladhar AM, Reid AT, Shumskaya E, de Laat KF, van Norden AG, van Dijk EJ, Norris DG, de Leeuw FE (2015): Relationship between white matter hyperintensities, cortical thickness, and cognition. Stroke 46:425–432.

Tzourio-Mazoyer N, Landeau B, Papathanassiou D, Crivello F, Etard O, Delcroix N, Mazoyer B, Joliot M (2002): Automated anatomical labeling of activations in SPM using a macroscopic anatomical parcellation of the MNI MRI single-subject brain. Neuroimage 15:273–289.

Uda S, Matsui M, Tanaka C, Uematsu A, Miura K, Kawana I, Noguchi K (2015): Normal development of human brain white matter from infancy to early adulthood: a diffusion tensor imaging study. Dev Neurosci 37:182–194.

Van Roon D, Caeyenberghs K, Swinnen SP, Smits-Engelsman BC (2008): Development of feedforward control in a dynamic manual tracking task. Child Dev 79:852–865.

Wu M, Lu LH, Lowes A, Yang S, Passarotti AM, Zhou XJ, Pavuluri MN (2014): Development of superficial white matter and its structural interplay with cortical gray matter in children and adolescents. Hum Brain Mapp 35:2806–2816.